

PROCEEDINGS OF SPIE

[SPIDigitalLibrary.org/conference-proceedings-of-spie](https://spiedigitallibrary.org/conference-proceedings-of-spie)

Extending wavefront sensing range of phase diversity

Zhaojun Yan, Pengqian Yang

Zhaojun Yan, Pengqian Yang, "Extending wavefront sensing range of phase diversity," Proc. SPIE 11057, Modeling Aspects in Optical Metrology VII, 110570W (21 June 2019); doi: 10.1117/12.2525980

SPIE.

Event: SPIE Optical Metrology, 2019, Munich, Germany

Extending Wavefront Sensing Range of Phase Diversity

Zhaojun Yan^{*a}, Pengqian Yang^b

^aDivision of Optical Astronomical Technologies, Shanghai Astronomical Observatory, Chinese Academy of Sciences, Shanghai 200030, China; ^bJoint Laboratory for High Power Laser Physics, Shanghai Institute of Optics and Fine Mechanics, Chinese Academy Sciences, Shanghai 201800, China

Phase diversity is a powerful methodology technique for measuring the wavefront aberrations of optical systems and surfaces by solving an unconstrained optimization problem from multiple images whose pupil phases differ from one another by a known amount. However, it often fails for large wavefront aberrations. A modified phase diversity technique to improve the sensing dynamic range was proposed. We conducted computer simulations of the reconstruction of large aberrations of an optical system with the proposed phase diversity method. We fitted the wavefront to Zernike polynomials to reduce the number of variables. The limited-memory Broyden-Fletcher-Goldfarb-Shanno (L-BFGS) algorithm was used for optimizing process. The study shows that the method can extend the dynamic range from about 2λ to about 11λ and the paper gives practical guidelines for the application of phase diversity methods to characterize large wavefront aberrations.

Keywords: phase diversity, wavefront sensing, L-BFGS, optimization problem

1. Introduction

Phase aberrations arise from a variety of sources including atmospheric turbulence, misalignments among optical elements, improper mirror figure and off-axis design residual^[1]. As a result, wavefront sensor is required to measure the aberrated wavefront and provide appropriate error signals to the actuator system to remove aberrations. Phase diversity, as a candidate wavefront sensing technique, first proposed by Gonsalves^[2], could detect phase aberrations from several images directly. This technique has already been used to check the alignment of optical systems and deconvolve aberrated images for about 35 years^[3,4]. It offers certain advantages over other wavefront sensors: the optical hardware required is simple to implement and it works well with extended objects^[5].

However, large aberrations with phase Peak Valley(PV) values higher than 2π might be encountered. In such a case, the data used in phase diversity do not contain the full information of the aberrated pupil phase. So, there are many equivalent solutions corresponding to both local optimums and the global one in the optimizing process.

In this paper, we used a modified phase diversity technique to extend the dynamic range of phase diversity. We conducted computer simulations of the reconstruction of large aberrations of an optical system with the phase diversity method. This paper explained how to extend the detecting range of phase diversity and discussed the results.

2. ESTIMATION OF ABERRATIONS BY PHASE DIVERSITY

2.1 Principle of phase diversity

Figure 1 illustrates the phase diversity principle^[6,7]. The idea of phase diversity is to collect at least two images that differ from each other by a known phase variation. The first is often the conventional focal-plane image that is degraded

by the unknown aberrations. Additional images of the same object are formed by perturbing these unknown aberrations in some known fashion. For example, a simple beam splitter and a second detector array that is translated along the optical axis, as depicted in Fig.1, constitutes a second imaging channel that produces a diversity image subject to the same unknown aberrations found in the conventional image, but is additionally impacted by a known amount of defocus.

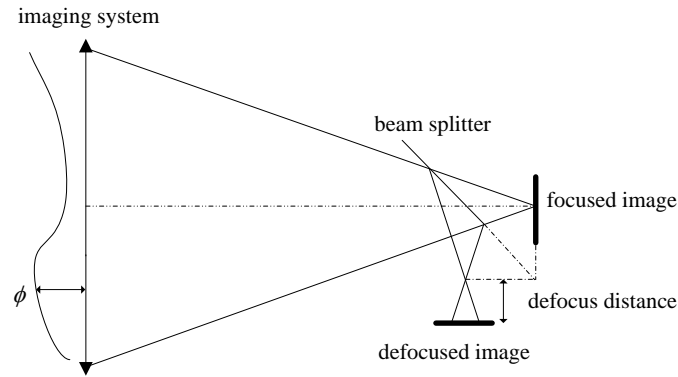


Fig. 1 Principle of phase diversity

The PD technique has been successfully used by some authors to determine aberrations^[8,9,10] and also to restore images^[11,12]. It uses a low-cost, optically simple wave-front sensor that consists of the imaging camera system, but requires a complex numerical and iterative processing to restore the unknown aberrations from the images.

2.2 Imaging model

In Fig.1, the input-output relationship for the optical system is described by the following equation:

$$d_k(x) = o(x) * h_k(x) + n_k(x) \quad . \quad (1)$$

Where k indicates the different optical channels, $o(x)$ indicates the object, $*$ indicates the convolution product, $n_k(x)$ denotes an additive noise and $h_k(x)$ is the point spread function (PSF) in optical channel k , which can be computed by:

$$h_k(x) = \left| \mathbf{F}^{-1} \{ P_k(u) \} \right|^2 \quad . \quad (2)$$

Where $\mathbf{F}^{-1} \{ \}$ indicates inverse Fourier transform, u is a two-dimensional vector in the pupil plane, and P_k is the generalized pupil function of channel k :

$$P_k(u) = |P_k(u)| \exp \{ i[\phi(u) + \Delta\phi_k(u)] \} \quad . \quad (3)$$

Where $\phi(u)$ is the unknown wave-front aberration that we would like to estimate. The phase function is expanded on a set of polynomials. Indeed, aberrations in an optical system can be mathematically represented by Zernike polynomials^[13].

$$\phi(u) = \sum_{i=4} a_i Z_i(u) \quad . \quad (4)$$

Where $\Delta\phi_k(u)$ is the known phase function introduced in the k -th optical channel. In our case, $\Delta\phi_k(u) = a_4^d Z_4(u)$ where Z_4 is the defocus Zernike polynomial. The choice of the known defocus distance is essential to obtain accurate

results. The RMS defocus coefficient a_4^d depends on the defocus distance d of the defocus channel, the telescope diameter D and the focal length F through:

$$a_4^d = \frac{\pi d}{8\sqrt{3}\lambda(F/D)^2} \text{ (in radian)} \quad (5)$$

The corresponding peak-to-valley optical path Δ is equal to

$$\Delta = \frac{\sqrt{3}\lambda a_4^d}{\pi} = \frac{d}{8(F/D)^2} \quad (6)$$

2.3 Aberration estimation principle

If an additive Gaussian noise model is adopted, the object $o(x)$ and the wave-front aberration function $\phi(u)$ can be computed by minimizing the cost function:

$$E = \sum_k \sum_x |d_k(x) - o(x) * h_k(x)|^2 \quad (7)$$

Using Parseval's theorem and the convolution theorem E can be expressed in the frequency domain:

$$E = \sum_k \sum_f |D_k(f) - O(f) \cdot H_k(f)|^2 \quad (8)$$

Where $D(f)$, $O(f)$, $H(f)$ are the Fourier transforms of $d(x)$, $o(x)$, $h(x)$ respectively.

Since several features make the inverse problem very difficult to solve, the problem is ill posed. Hence, we add regularization terms to obtain the modified cost function:

$$E_M = \sum_k \sum_f |D_k(f) - O(f) \cdot H_k(f)|^2 + \gamma \sum_f |O(f)|^2 \quad (9)$$

Setting $\partial E_M / \partial O$ to zero, we obtain the solution of $O(f)$:

$$O(f) = \frac{\sum_k D_k H_k^*}{\sum_k |H_k|^2 + \gamma} \quad (10)$$

Substituting equation (10) back into equation (9), we obtain the cost function:

$$E_M = \sum_k \sum_f |D_k|^2 - \sum_f \frac{\left| \sum_k D_k H_k^* \right|^2}{\sum_k |H_k|^2 + \gamma} \quad (11)$$

Then the unknown wave-front aberration can be estimated by minimizing the cost function with the help of optimization methods. An analytic expression for the derivative of the cost function with respect to the aberration parameters is given by:

$$\frac{\partial}{\partial a_i} E_M = \frac{4}{N^2} \sum_u Z_i(u') \text{Im} \left[\sum_{k=1} H_k(u') (\mathbf{T}_k * H_k^*)(u') \right] \quad (12)$$

Where

$$\mathbf{T}_k(u) = \frac{\left[\sum_l |H_l|^2 (\sum_j D_j H_j^*) D_k^* - \left| \sum_j D_j H_j^* \right|^2 H_k^* \right]}{(\sum_l |H_l|^2 + \gamma)^2} \quad (13)$$

Note: the size of object $o(x)$ is $N \times N$ and the operator $\text{Im}[\cdot]$ takes the imaginary part of the argument.

The cost function in Eq. (13) is minimized with respect to a set of unknown phase parameters by a nonlinear optimization routine such as steepest descent, conjugate gradient, Newton or quasi-Newton, simulated annealing, or even genetic algorithms. Limited memory quasi-Newton methods are useful for solving large-scale optimization problems. L-BFGS algorithm is very well suited to PD, due to its efficiency and good performance in solving large-scale optimization problems.

2.4 Defocus distance effect

The corresponding defocus distance depends on the focal ratio of the optical system. When the defocus distance decreases, the difference between the focal image and the defocus image is no longer sufficient to allow for a good convergence of the phase diversity algorithm. The old view that when the defocus distance is too large, the contrast in the out of focus image is attenuated and this image was no longer usable so that the defocus distance around the value (typically $\lambda \pm \lambda/2$) would provide accurate results which was shown in the former study^[14]. However, we did some research on the effect of defocus distance and obtained some new interesting results.

3. SIMULATION RESULTS

In this section, we show simulation results of measuring the simulated aberrations based on the phase-diversity method. We generated a complex pupil function using a uniformly illuminated circular pupil of diameter 28 mm paired with a varying phase function shown in Fig.2. The phase function contains mostly spherical aberration and some small asymmetric aberrations. The RMS and PV of the aberrated phase is 1.807λ and 10.961λ respectively. The pupil function was applied to an f/25 lens with a focal length of 700 mm.

The conditions for the simulations are given by a point object, an imaging wave-length of 632.8 nm and a pure defocus (has different PV value) between the two images. The computational domain is taken to be a 1024×1024 pixels array and then the two intensity images were computed. The simulated pixel pitch of the camera is 6.45 μm . The input images are Nyquist sampled^[15] in this simulation condition. No noise is considered here. Then we can apply PD algorithm. Piston, tip or tilt terms are not included in the reconstructed results since they cannot be estimated by phase diversity.

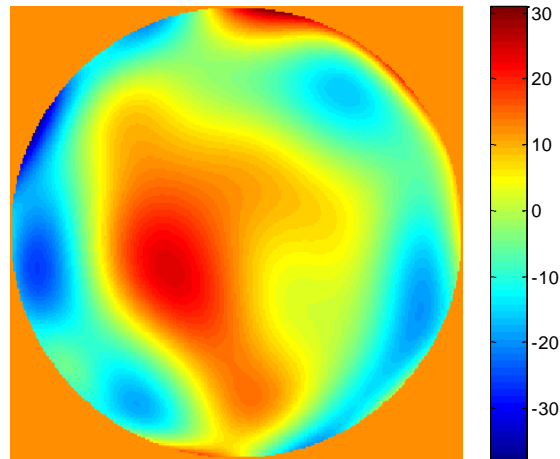


Fig.2. Phase function (in radians) used to generate intensity images

3.1 Results of experiment 1

In experiment 1, the RMS of the induced defocus aberration is 5 radians. Fig.3 and Fig.4 show a comparison between the input focus and defocus images and the reconstructed focus and defocus images aberrated by the estimated phase. Fig. 5 quantifies the convergence performance of the PD algorithm. The input and reconstructed phase results are shown in Fig.6. Fig. 6 (c) shows that the residual wavefront RMS is 2.2λ which means the input aberration cannot be reconstructed successfully in this simulation experiment.

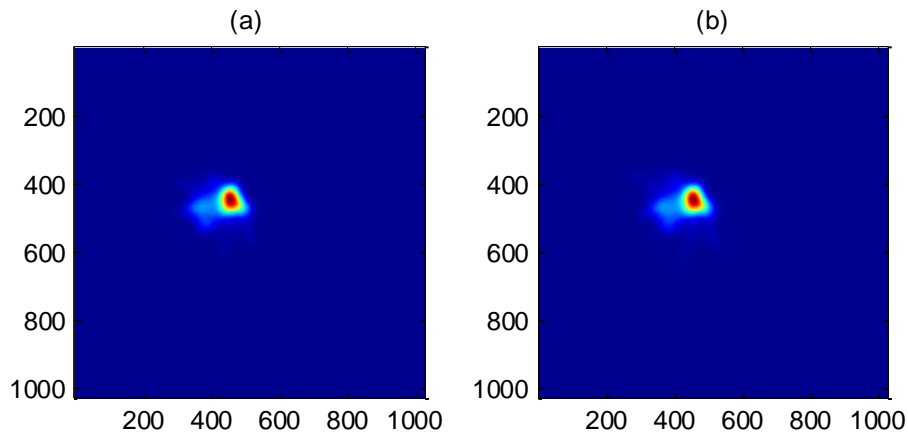


Fig.3. Comparison between measured focus image (a) and reconstructed focus image (b)

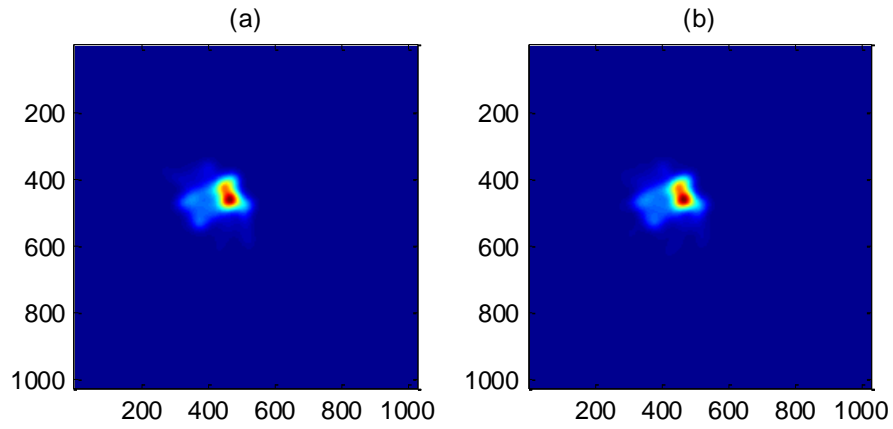


Fig.4. Comparison between measured defocus image (a) and reconstructed defocus image (b)

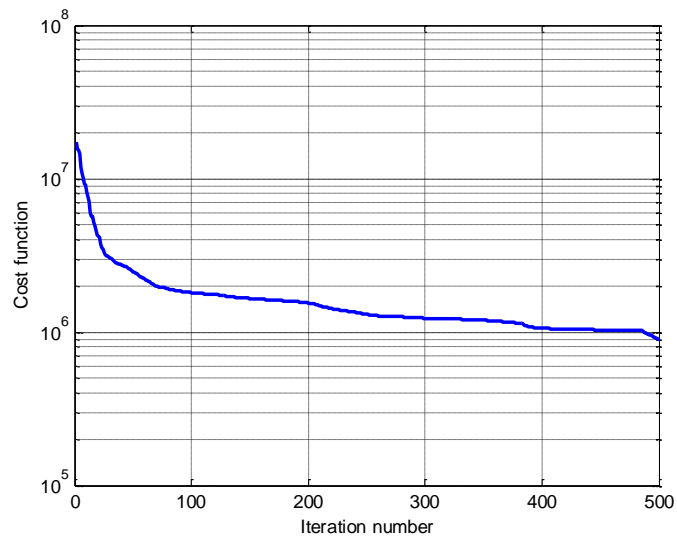


Fig.5. Cost function versus number of iterations

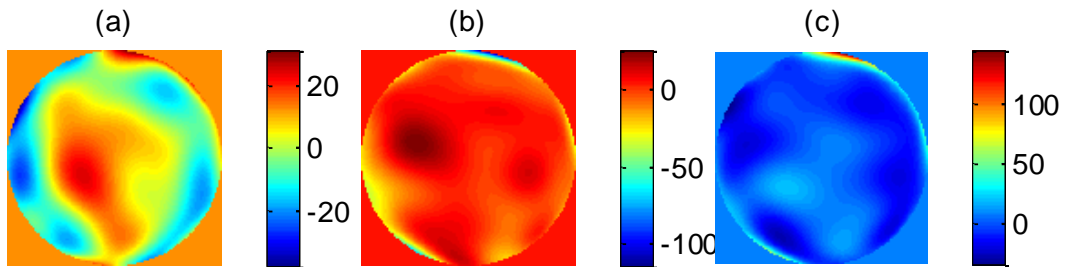


Fig.6. The input aberration (a), the reconstructed aberration (b) and the residual reconstructed aberration (c) (Phases are shown in radians)

3.2 Results of experiment 2

In experiment 2, the RMS of the induced defocus aberration is 20 radians. Fig.7 shows a comparison between the input defocus image and the reconstructed defocus images. Fig. 8 quantifies the convergence performance of the PD algorithm. The comparison between the induced aberration and the reconstructed results are shown in Fig.9. Fig. 9 (c) shows the residual wavefront RMS is $3.51 \times 10^{-6} \lambda$ that means the aberration is reconstructed successfully in this simulation experiment. Fig. 10 quantifies the performance of wave-front estimation by comparing the input and estimated Zernike coefficients. These results show that the PD algorithm performs well when the defocus aberration is 20 radians which is greater than the induced defocus aberration in the first experiment.

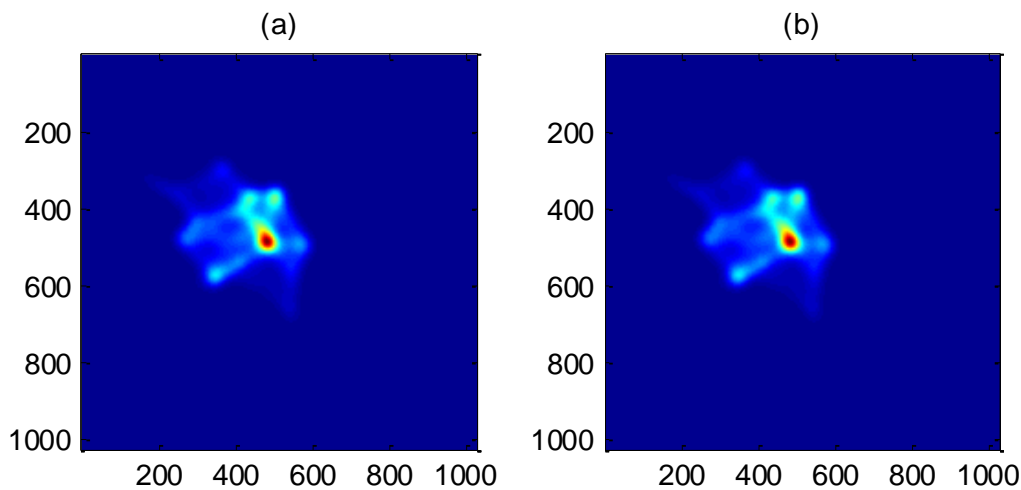


Fig.7 Comparison between measured defocus image (left) and reconstructed defocus image (right)

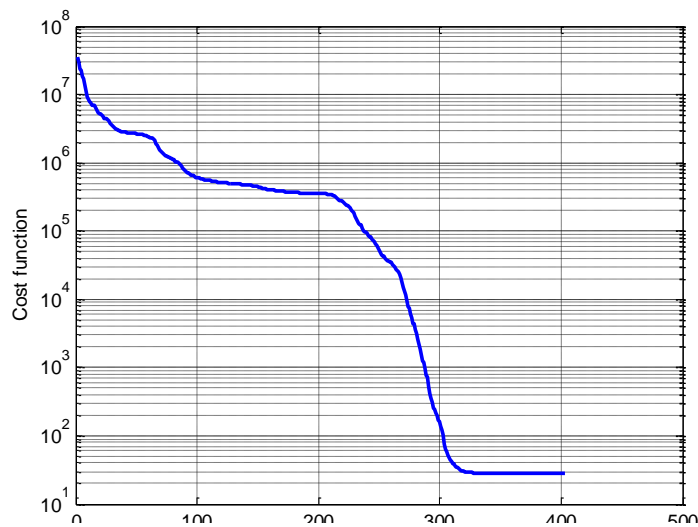


Fig.8. Cost function versus number of iterations

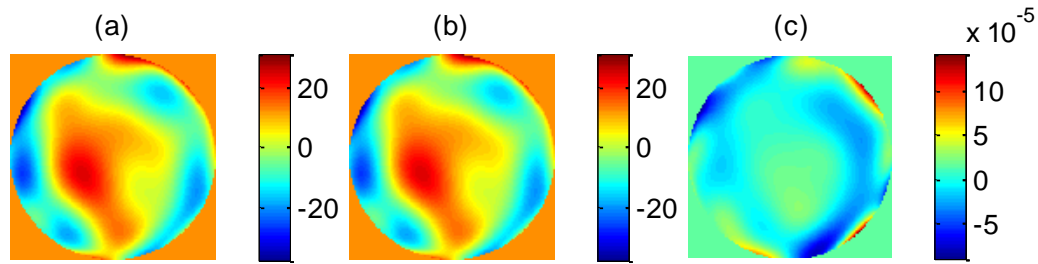


Fig. 9 The input aberration (a), the reconstructed aberration (b) and the residual reconstructed aberration (c) (Phases are shown in radians)

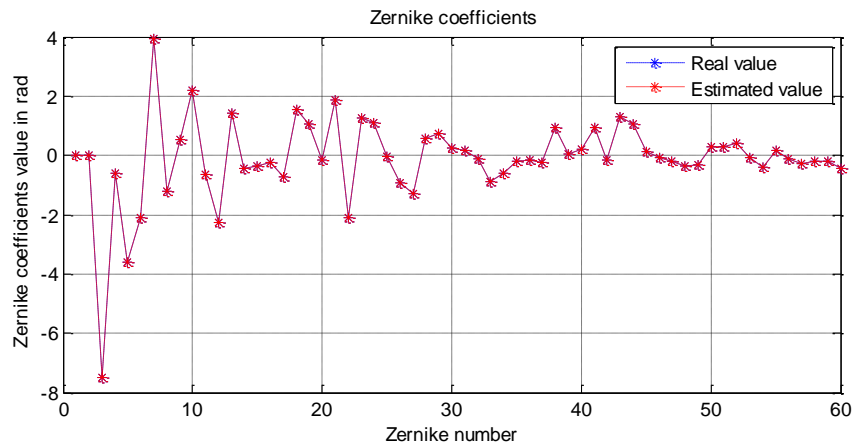


Fig. 10 Comparison between true and estimated Zernike coefficients

3.3 Results of experiment 3

In experiment 3, we increased the RMS value of the induced defocus aberration to 30 radians. Fig. 11 (c) shows the residual wavefront RMS is $2.4 \times 10^{-6} \lambda$. Fig. 12 shows the algorithm begins to converge after 180 iterations. However, Fig. 8 shows that the algorithm begins to converge after 400 iterations in experiment 2. By comparing the algorithm convergence in experiment 1, 2 and 3, the known amount of defocus really impacts the convergence rate and the phase reconstruction precision. The larger the defocus, the greater difference between the focus and defocus images, the better reconstruction results could be obtained. On the other hand, the larger the defocus, the larger size of the defocus image, and we need more memory to save images and more time to do the Fourier transformation calculation in the optimizing process. All things considered, we should select an appropriate value of the defocus distance.

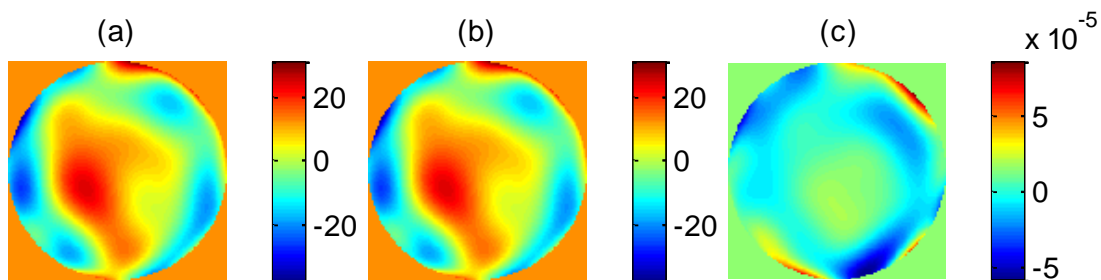


Fig. 11 The input aberration (a), the reconstructed aberration (b) and the residual reconstructed aberration (c) (The units are in radians)

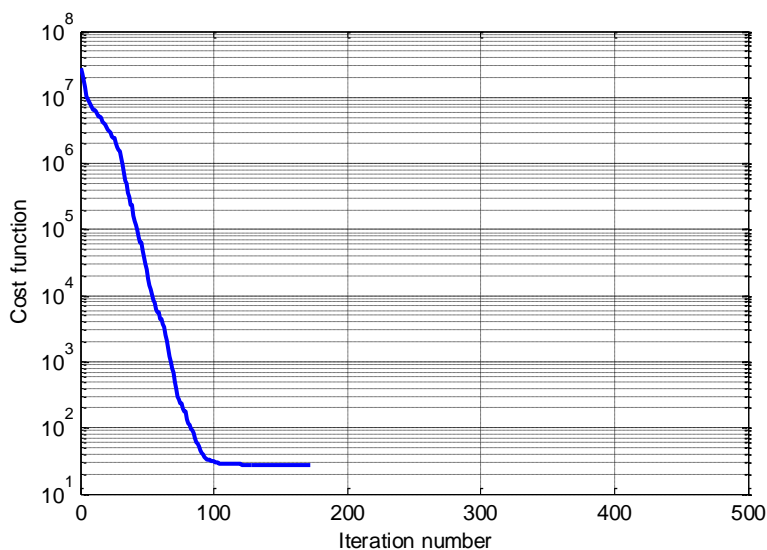


Fig. 12 Cost function versus number of iterations

4 CONCLUSIONS

We have given a precise description of the phase diversity algorithm and its usage for the estimation of aberrations. Several simulated examples with different amount of induced defocus have been proposed in order to investigate its effect on the dynamic range of the phase diversity algorithm. This study highlights a certain amount of defocus aberration needed to be generated to obtain accurate results and shows that the phase diversity algorithm can have large dynamic range up to about 11λ . In the near future, we will do the relative experiments for further validation. General, for future high performance optical detection, this method may be of interest to achieve the challenging science goals of the optical community.

REFERENCES

- [1]. Scharmer, G. B., Löfdahl, M. G., van Werkhoven, T. & de la Cruz Rodriguez, J..2010, *Astronomy & Astrophysics* 521, A68
- [2]. R. A. Gonsalves. *Optical Engineering*, 1982, 21(5): 829-832

- [3]. Mats G. Lofdahl, Richard L. Kendrick, et al. SPIE, 3356:1190-1201
- [4]. Mats G.Lofdahl, Goran B.Scharmer. SPIE, 1994, 2302: 254—267
- [5]. Richard G.Paxman, Brian J. Thelen, Ryan J.M urphy, et al. SPIE 2007, 6711:671103
- [6]. Gonsalves, R. A. 1982, Opt. Eng., 21, 829
- [7]. Paxman, R. G., Schulz, T. J., & Fienup, J. R. 1992, J. Opt. Soc. Am. A, 9, 1072
- [8]. Carreras, R. A., Restaino, S., & Duneman, D. 1994, SPIE, 2302, 323
- [9]. Lee, D., Welsh, B., & Roggemann, M. 1997, Opt. Lett., 22, 952
- [10]. Thelen, B. J., Paxman, R. G., Carrara, D. A., & Seldin, J. H. 1999, J.Opt. Soc. Am. A, 16, 1016
- [11]. Restaino, S. 1992, Appl. Opt., 31, 7442
- [12]. Seldin, J., & Paxman, R. 2000, in Imaging Technology and Telescopes, SPIE, 4091-07
- [13]. Noll, R. J. 1976, J. Opt. Soc. Am., 66(3), 207
- [14]. Meynadier, L., Michau, V., Velluet, M.-T., et al. 1999, Appl. Opt., 38, 4967
- [15]. Jefferies, S. M., Lloyd-Hart, M., Keith Hege, E., & Georges, J. 2002, App. Opt., 41, 2095